frontiers | Frontiers in Built Environment

TYPE Original Research
PUBLISHED 04 May 2023
DOI 10.3389/fbuil.2023.1137569

OPEN ACCESS

EDITED BY
Paul Awoyera,
Covenant University, Nigeria

REVIEWED BY
Humphrey Danso,
Akenten Appiah-Menka University of Skills Training and Entrepreneurial Development, Ghana
Shaker Qaidi,
University of Duhok, Iraq

*CORRESPONDENCE
Xuefeng Xu,
raymond_xu@my.swjtu.edu.cn

SPECIALTY SECTION
This article was submitted to Construction Materials, a section of the journal Frontiers in Built Environment

RECEIVED 04 January 2023
ACCEPTED 06 March 2023
PUBLISHED 04 May 2023

CITATION
Xie W, Xu X, Xu C, Tian F, Mao Q, Li H, Liu L and Qin G (2023), An experimental study and axial tensile constitutive model of the toughness of PP-SACC for rapid repairs. *Front. Built Environ.* 9:1137569. doi: 10.3389/fbuil.2023.1137569

An experimental study and axial tensile constitutive model of the toughness of PP-SACC for rapid repairs

Wen Xie[1], Xuefeng Xu[2]*, Chunlei Xu[1,2], Feng Tian[1], Qiwen Mao[1], Helong Li[1], Lin Liu[1] and Gongyi Qin[1]

[1]China Nuclear Industry Huachen Construction Engineering Co., Ltd., Xi'an, Shaanxi, China, [2]Institute of Civil Engineering Materials, School of Civil Engineering, Southwest Jiaotong University, Chengdu, China

To improve the economic benefits of engineered cementitious composites and control the repair cycle, repair materials were designed, with the key components of the mixture being low-cost polypropylene (PP) fibers and fast-setting sulfoaluminate cement. The effects of water/binder ratio, fiber content, and aggregate particle size on the flowability, mechanical properties, and toughness of the polypropylene fiber-reinforced sulfoaluminate cementitious composite (PP-SACC) were explored. Based on experimentally measured axial tensile stress–strain curves, a constitutive model of PP-SACC was derived in terms of fiber content and water/binder ratio. Additionally, the correlation coefficients representing the relationships of the mixture indices with the tensile properties were explored based on revised gray relational analysis. Test results indicated that fiber content and water/binder ratio were the most important factors affecting the mechanical properties, toughness, and fluidity of the material; in contrast, the influence of aggregate size was slight. The PP-SACC mixture with an aggregate size of 75 μm, a water/binder ratio of 0.30, and a fiber content of 3.0% demonstrated an excellent degree of toughness and exhibited a flexural hardening phenomenon under bending load.

KEYWORDS

PP fiber-reinforced sulfoaluminate cementitious composite, axial tensile constitutive model, tensile strain, multiple cracks, flexural toughness

1 Introduction

Since the 1990s, cement mortar and cement concrete have been widely used in construction, including in highways, bridges, ports, and other domains, where they have played a critical role because of advantages such as easy access to raw materials, low price, high strength, durability, and convenience (Yesudhas Jayakumari and Nattanmai Swaminathan, 2023). Cement-based materials are still the world's most widely used building materials. However, due to the inherent shortcomings of cement-based

Abbreviations: PP, polypropylene; PP-SACC, polypropylene fiber-reinforced sulfoaluminate cementitious composite; SACC, sulfoaluminate cement-based composite; PVA, polyvinyl alcohol; PE, polyethylene; SAC, sulfoaluminate cement; HRWRA, high-range water-reducing admixture; W/B, water/binder ratio; LVDT, linear variable differential transformer.

materials, inadequate design, and a lack of maintenance of the structure, most of the early concrete structures built in China have faced problems with strengthening and repair. The maintenance cost of infrastructure has become a major problem, which has led to a sharp increase in the total cost over the entire life cycle of the structure. The restoration and reinforcement of existing cement concrete structures has attracted extensive attention in the engineering field.

Repair materials can be divided into organic and inorganic composites based on their components. Organic repair materials (Wang et al., 2020; Lee, 2021) are often used in pavement repair due to their high impermeability, corrosion resistance, early high strength, fast curing characteristics, and other advantages. However, there are also problems with these materials, such as a significant difference between the elastic modulus of the repair materials and the old concrete, and the ease with which they can separate from the surface of the old concrete and fall off (Elsanadedy et al., 2019). Modified organic repair materials mainly involve the incorporation of polymers into cement-based materials to cement hydration products and aggregate them together by attaching to hydration products, thereby improving bonding performance, material toughness, and interface microstructure (Sadrmomtazi and Khoshkbijari, 2017; Chen et al., 2021). However, due to the limited number of polymer varieties available, the high price of raw materials, and the limitations of preparation technology, most ordinary repair projects cannot afford to use this type of material and its application is limited (Siddika et al., 2021). Inorganic repair materials are modified by adjusting the water–binder ratio of ordinary Portland cement or mixing in inorganic fibers (Afroughsabet et al., 2016; Cao et al., 2020; Sakr et al., 2021). Cement-based repair materials have good deformation compatibility and volume stability due to their similar properties and structure compared to old concrete materials, and so they are used as the primary repair materials in repair engineering. However, these materials also have problems, such as low bond strength, high shrinkage rate, and high brittleness (Belaidi et al., 2015). As a reinforced composite material, fiber is widely used in cement mortar systems, and it can make up for these defects. Not only can the use of fiber-reinforced inorganic repair materials improve the brittleness of repair materials through the addition of fiber, but this can also improve bond strength (Soupionis et al., 2020). Since its introduction, one of the main applications of strain-hardened cement-based composite (SHCCs), also known as engineered cementitious composite (ECC), has been in the repair of existing concrete structures. Xu and Zhang (2012) found that, as a repair material, ECC can effectively prevent interface cracks and avoid standard failure modes in repair systems such as spalling and cracking. An ECC repair system has more substantial ductility and a greater energy absorption capacity, and provides good control over crack width (Shilang et al., 2011). ECC can effectively reduce crack width and redistribute the internal forces of the repaired structural system (Xu and Wang, 2011). Wu and Li (2017) conducted an experimental study on a repair system constituted by pouring UHTCC on the bending side of an ordinary concrete beam body and found that adding UHTCC on the surface improved the strength of the repair system and inhibited the development of cracks.

In restoration engineering, rapid hardening, high early strength, and high toughness are very high priorities for the preparation of restoration materials. Due to the long curing period of ordinary Portland cement-based repair materials, these are unsuitable for urgent repair works. However, the repair period can be significantly shortened through the use of a sulfoaluminate cement-based composite (SACC) (Hu et al., 2019). In addition, polyethylene (PE) fiber and polyvinyl alcohol (PVA) fiber, which are commonly used in ECC materials, are often limited in their use in civil engineering due to their high prices (Kang et al., 2018). Polypropylene (PP) fiber, which provides good performance at a reasonable price, has great potential for applications in repair materials.

Among the various cements available for concrete, sulfoaluminate cement (SAC)-based binders have attracted a great deal of attention. SAC meets many essential requirements for these applications, namely, it is quick setting and develops high early strength (Kong et al., 2022). As a rapid-hardening cement, SAC has been increasingly used for building in cold regions and in repair structures due to its notable properties such as high early strength, freezing resistance, and low permeability and alkalinity (Cai and Zhao, 2016). Additionally, SAC production is associated with lower carbon dioxide emissions than PC production (Zhen et al., 2021). Tayeh et al. investigated the effects of three types of steel fibers (straight, hooked, and corrugated), with varying volume fractions of steel fibers (0.75%, 1.5%, and 2.5%), on the fresh and mechanical properties of ultra-high-performance concrete (Tayeh et al., 2022a; Tayeh et al., 2022b). The results indicated that the use of deformed fibers and an increased fiber volume gradually reduced the flowability of UHPC. Fiber use also had a significant impact on the compressive strength and fracture modulus of UHPC. Furthermore, the authors studied the effect of microsilica and polypropylene fibers (PFs) on the mechanical properties of ultra-high-performance geopolymer concrete (UHP- GPC). A total of 20 concrete mixtures were evaluated experimentally for workability, compressive strength, elastic modulus, and splitting tensile strength. The results showed that the mechanical properties were significantly degraded when 15% microsilica was added to UHP-GPC, but improved when microsilica was added at proportions greater than 15% (Abu Aisheh et al., 2021; Abu Aisheh et al., 2022).

However, there is relatively little research on PP fiber-reinforced sulfoaluminate cement as a repair material, and the factors influencing the properties of repair materials still need to be clarified and a more complete understanding developed. Zhang et al. (2021) studied the mixing of PP and PVA fibers to explore the mechanisms underlying the influence of fiber content on various performance indices of repair materials. Li (2018) studied the effects of mineral admixture type, PP fiber content, and water-reducing agents on Portland cement-based repair materials. He et al. (2019) prepared an ECC material by adding PVA fiber-reinforced sulfoaluminate cement and explored the optimal dosage of PVA and its strengthening mechanism. On the basis of this previous work, this paper comprehensively considers the combined demands of low cost, early strength, and toughness in an examination of the advantages of sulfoaluminate cement and polypropylene fiber. A four-point sheet metal test was conducted to study the mechanical properties and flexural toughness of PP-SACC. The multi-factor influence of critical indicators of materials was evaluated using gray

TABLE 1 Properties of the cement and cenospheres.

Property		Sulfoaluminate cement	Cenosphere
Chemical composition (% by mass)	SiO_2	9.7	56.5
	CaO	47.0	4.8
	MaO	4.0	1.3
	Al_2O_3	23.0	26.5
	Fe_2O_3	2.3	5.3
	SO_3	12.0	0.7
	Na_2O	—	1.4
	K_2O	—	3.3
Physical properties	Specific surface area (m^2/kg)	418	—
	Initial setting time (min)	39	—
	Final setting time (min)	53	—

correlation analysis, providing guidance for further promotion of the applications of high-performance restorative materials.

2 Significance of the research

ECC, which is characterized by high ductility and high performance, has been investigated extensively in recent years. However, the application of ECC in practical engineering is still constrained. On the one hand, the high cost of ECC is a key problem that has constrained its application, as PVA fiber is generally costly and difficult to obtain. On the other hand, the use of environmentally friendly products has become an important principle in local construction. Currently, cement-based repair materials are generally made with ordinary Portland cement, which not only leads to a long repair cycle and means that maintenance takes a long time, but also produces high CO_2 emissions. Sulfoaluminate cement has major advantages in construction repair due to its early strength and rapid hardening. To reduce the shrinkage of sulfoaluminate cement, the incorporation of PP fiber is generally considered an effective method. Furthermore, as a relatively cheap and practical modification component, PP fiber has significant advantages in inhibiting shrinkage and improving toughness. Therefore, the investigation of PP fiber-reinforced sulfoaluminate cementitious composites is of great importance in maintenance engineering. Not only can the successful application of PP-SACC improve repair speed, but it also greatly reduces economic costs.

3 Materials and experimental design

3.1 Materials

The materials employed in the experimental tests were as follows: cement (42.5 sulfoaluminate cement; chemical composition and physical indices are presented in Table 1); cenospheres (chemical composition is shown in Table 1); quartz sand, adopted as a fine aggregate at two different particle sizes (75 μm and 109–212 μm); and polypropylene (PP) fiber, employed as an additive at 2.5% and 3.0% content by total volume. A high-range water-reducing admixture (HRWRA) with a water-reducing rate of 40% was also used.

3.2 Design of the mix proportion

An experimental program was designed to investigate the influence of the water/binder ratio (*W/B*), aggregate size, and fiber content on the mechanical properties, toughness, and fluidity of PP-SACC. Cenospheres, as the highest value-added fractions of coal fly ash, were added to PP-SACC for workability reasons. The incorporation of cenospheres can significantly increase the mix viscosity of the paste due to their hollow spherical structure. Furthermore, cenospheres can also improve the compactness of hardened composites, especially in the transition zone between aggregate and cement paste. Therefore, cenospheres were added to PP-SACC at a content ratio of 20% of the binder. The sand/binder ratio was fixed at 0.36. The bulk density was 2072 kg/m^3. The overall mix proportions are presented in Table 2. Existing research results have indicated that even when the fiber content reaches 2.5%, PP composites do not present the expected behavior of an ECC. In fact, the rheology of the paste is important for uniform fiber distribution to obtain the desired mechanical properties. In this study, the addition of superfine quartz sand and the adoption of HRWRA made it possible to test higher levels of fiber content, i.e., 2.5% and 3.0%, in ECC (Ehrenbring et al., 2022; Hou et al., 2022; Tan et al., 2023).

3.3 Experimental methods

3.3.1 Casting and molding

First, binder (sulfatealuminate cement and cenospheres) and aggregates were poured into a mixer for homogenization. Subsequently, water premixed with HRWRA was added. Finally,

TABLE 2 Mix proportions of PP-SACC materials.

Mix ID	W/B	Aggregate size	Vf (%)	S/B
A'-2.5	0.40	75 μm	2.5	0.36
A'-3.0	0.40	75 μm	3.0	0.36
A-2.5	0.40	109–212 μm	2.5	0.36
A-3.0	0.40	109–212 μm	3.0	0.36
B'-2.5	0.30	75 μm	2.5	0.36
B'-3.0	0.30	75 μm	3.0	0.36
B-2.5	0.30	109–212 μm	2.5	0.36
B-3.0	0.30	109–212 μm	3.0	0.36
C'-2.5	0.25	75 μm	2.5	0.36
C'-3.0	0.25	75 μm	3.0	0.36
C-2.5	0.25	109–212 μm	2.5	0.36
C-3.0	0.25	109–212 μm	3.0	0.36

*A, B, and C represent three different water/binder ratios; A′, B′, and C′ with superscripts denote the use of the 75 μm aggregate and A, B, and C without superscripts denote the use of the 109–212 μm aggregate size. The subsequent numbers represent fiber volume content.

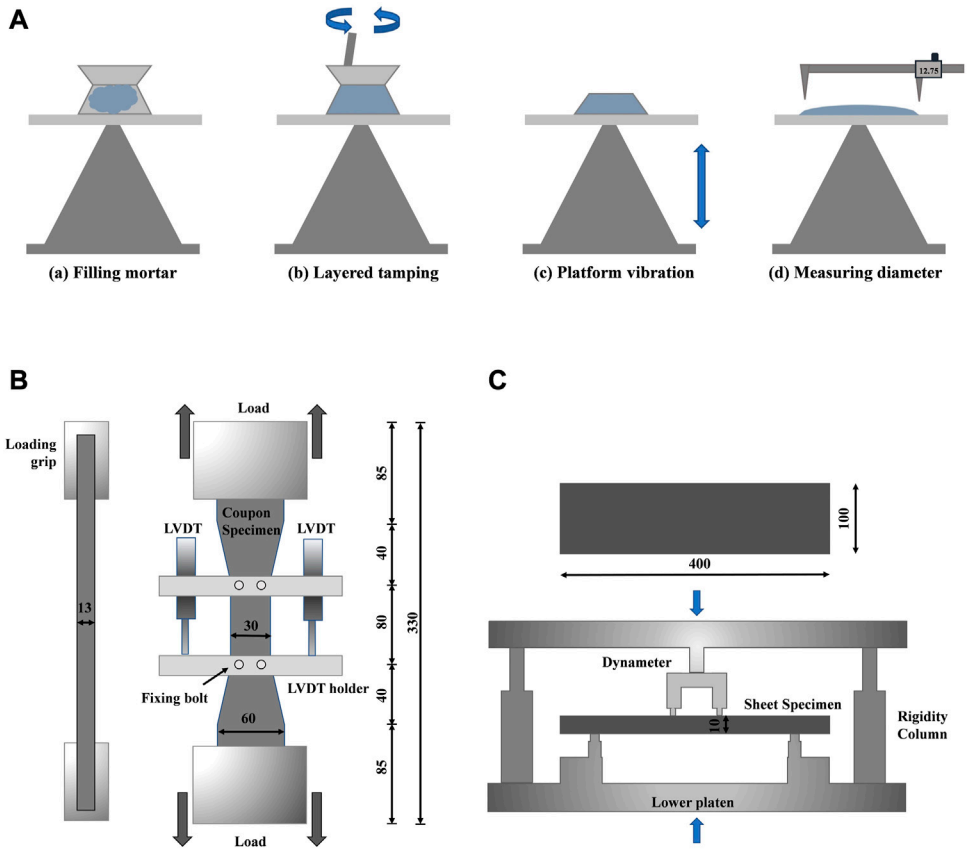

FIGURE 1
Schematic diagram of experimental equipment. **(A)** Cement mortar fluidity test. **(B)** Axial tensile test. **(C)** Four-point bending test.

PP fibers were sprinkled in and mixed until the fibers were uniformly dispersed in fresh paste. The fresh cement-based paste was then rapidly cast into molds. After 14 days of curing, an assessment of the mechanical properties was conducted.

3.3.2 Fluidity test

A fluidity test was conducted according to the relevant regulations of the "method for determination of fluidity of cement binder sand" (GB/T 2419-2005). As shown in Figure 1A, the point of contact between the instrument and the mortar was wiped with a wet cotton cloth. The mortar was then divided, mixed into two layers, immediately placed into a flow test die, and tamped 15 times. Then, the second mortar was filled and tamped 10 times. After the tamping was completed, the die sleeve was removed. Next, the Cutting cone circular die was slightly lifted in the vertical direction and the jumping table was immediately started. After the vibration process was complete, a caliper was used to measure the maximum diffusion diameter of the bottom surface of the mortar and its vertical diameter; the mean value was calculated, and this was taken to represent the fluidity of the cement mortar.

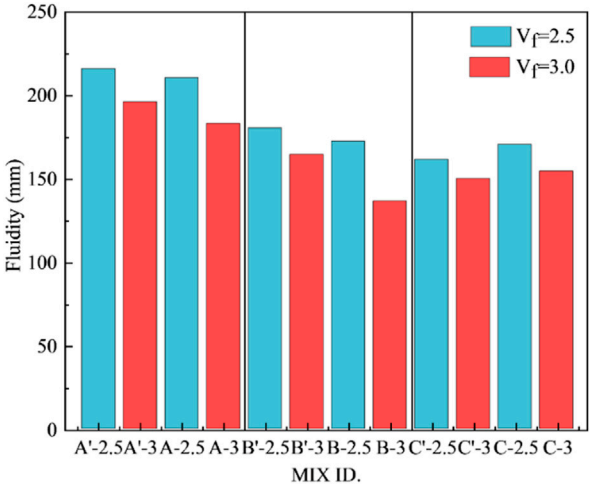

FIGURE 2
Summary of the fluidity of all mixtures.

3.3.3 Axial tensile test

A tensile test is the most direct method of verifying the strain-hardening behavior of PP-SACC. However, there are several problems in the process of conducting the test. At present, the fixing of a direct tensile specimen can be generally divided into methods of the clamping type and methods of the bonding type. Clamping methods are carried out using a specially designed fixture or a chuck clamp. To avoid slipping of the specimen during the test, a strong clamping force is generally applied to specimens. Therefore, reinforcement in the form of an aluminum paste plate or fiber cloth is frequently employed to protect the end of the specimen from breaking. However, in the clamping method, the end of the specimen is often the weak part in the tensile test and therefore results in a test failure. This is attributed to the nature of the multi-directional force applied to the end of the specimen. In bonding methods, both ends of the specimen are bonded with epoxy resin or another adhesive. The tensile stress of the fixture is transferred to the specimen through the adhesive. However, in order to ensure adhesive strength, the surface of the specimen usually needs to be ground, which may introduce initial cracks in the specimen before testing if this is done using improper methods. Furthermore, bonding methods are demanding in terms of the high requirement for alignment of the axis of the specimen in the installation process. Unsatisfactory alignment of the specimen will cause local stress concentration and eccentric tension of the specimen and thereby exert a negative impact on the test result.

Given these challenges, the axial tensile test employed in this study was conducted following the procedures specified in the JSCE (Japan) "Recommendations for Design and Construction of High-Performance Fiber Reinforced Cement Composites with Multiple Fine Cracks (HPDFRCCC)" (Yokota et al., 2008).

To determine the tensile strength and failure characteristics of the PP-SACC, dog-bone specimens of the material were prepared. The specimens were demolded after 24 h and placed in a standard curing room for 14 days. As shown in Figure 1B, an axial tensile test was performed using a closed-loop controlled material testing system at a loading rate of 0.1 mm/s. During the axial tensile test, the load and deformation values were recorded on a computerized data recording system. An extensometer was employed to measure the deformation of the specimen during the tensile test. On the stress–strain curve, the maximum stress was taken to represent the peak tensile stress, and the corresponding strain was taken to represent the peak strain.

3.3.4 Four-point bending test

A four-point bending test was applied following the CECS13: 2009 procedures of the "Standard test method for flexural toughness and first-crack strength of fiber-reinforced concrete" (CECS13: 2009).

The bending properties of PP-SACC were studied using sheet specimens. As shown in Figure 1C, the dimensions of each specimen were 400 mm × 100 mm × 10 mm. Four-point bending tests were performed at a loading rate of 0.5 mm/s. The span length of the flexural loading was 300 mm with a 100 mm center span length. During the flexural tests, the load and mid-span deflection were recorded on a computerized data recording system, and an LVDT was fixed on the test set-up to measure the flexural deflection of the specimen.

4 Experimental results and analysis

4.1 Analysis of fluidity

The fluidity of each mixture is summarized in Figure 2.

As indicated in Figure 2, the fluidity of PP-SACC decreased with increasing fiber content and aggregate size; however, the fluidity increased with an increase in water/binder ratio. Water/binder ratio was the most influential factor, followed by fiber content; aggregate size was the least influential. It can be noted in Figure 2 that the fluidity of mix A-2.5 (with 109–212 μm aggregate) was reduced by 2.5% in comparison with mix A′-2.5 (with 75 μm aggregate). The fluidity of mix A′-3.0 (with 3.0% fiber content) was reduced by 6.5%

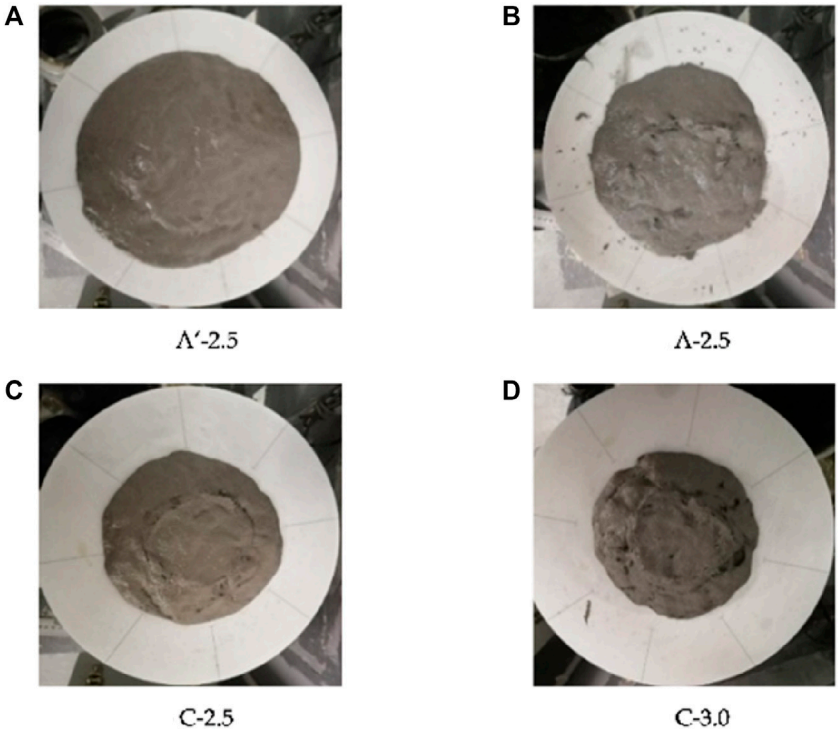

FIGURE 3
Fluidity test of Four Different Mix Proportions of PP-SACC. **(A)** A′-2.5 (W/B = 0.4, with 2.5% fiber content and 75 μm aggregate), **(B)** A′-2.5 (W/B = 0.4, with 2.5% fiber content and 109-212 μm aggregate), **(C)** C-2.5 (W/B = 0.25, with 2.5% fiber content and 109-212 μm aggregate), **(D)** C-3.0 (W/B = 0.25, with 2.5% fiber content and 109-212 μm aggregate).

in comparison with mix A′-2.5 (with 2.5% fiber content). Finally, the fluidity of mix B′-2.5 (with a water/binder ratio of 0.30) was increased by 16.4% in comparison with mix A′-2.5 (with a water/binder ratio of 0.25).

The effect of fiber content on fluidity was significant, as indicated in Figure 3. Mix A′-2.5 (flow diameter of 216 mm) exhibited a good fiber array in the paste. Furthermore, mix C-2.5 (with a flowability of 170.5 mm) generated no fiber alignment. However, when flowability was lower than 170 mm, such as in mix C-3.0 (flow diameter of 154.5 mm), it was difficult for the fibers in the paste to disperse and thereby trigger a decrease in fluidity. The fibers were distributed randomly in the paste and agglomerated in the network structure. This network structure may hinder the free flow of the paste, thereby affecting fluidity. Generally, fluidity decreases with increasing fiber content (Boulekbache et al., 2010). In addition, PP fibers can be wetted by the matrix and this can bond well with the fibers. However, when fiber content exceeds a critical point, fiber adhesion decreases. This may be attributed to an insufficient quantity of matrix to fully wet and bond to the fibers (Lu et al., 2018).

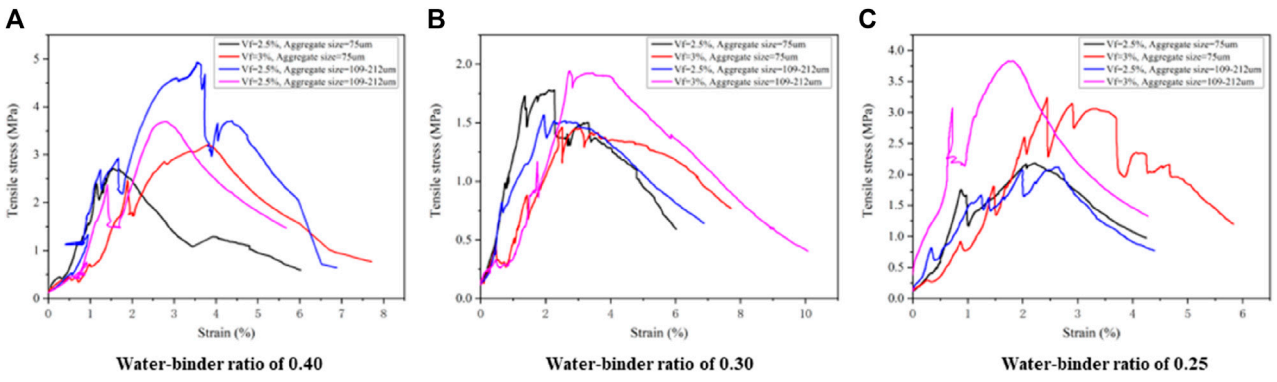

FIGURE 4
Tensile stress–strain curves of PP-SACC. **(A–C)** represent the working conditions of water cement ratio of 0.4, 0.3, and 0.25, respectively.

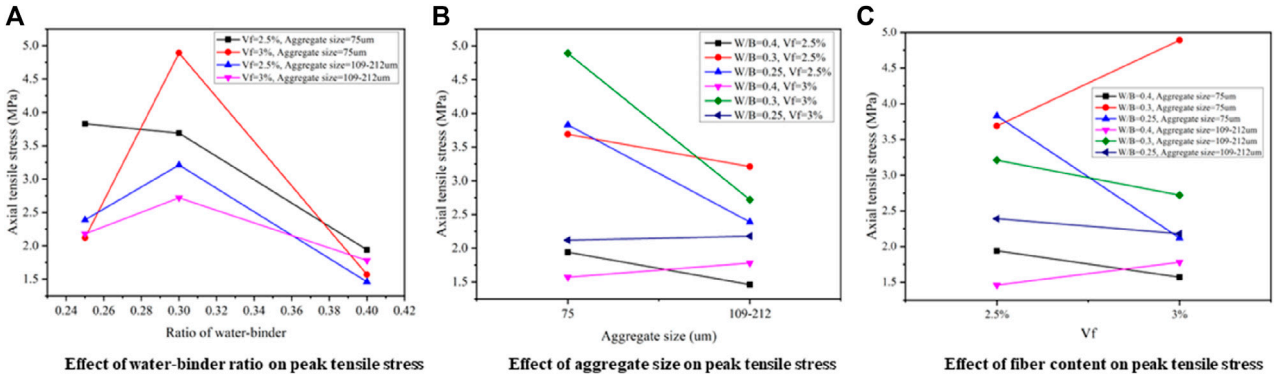

FIGURE 5
Effects of each factor on tensile strength. **(A)** Effect of water-binder ratio on peak tensile stress, **(B)** Effect of aggregate size on peak tensile stress, **(C)** Effect of fiber content on peak tensile stress.

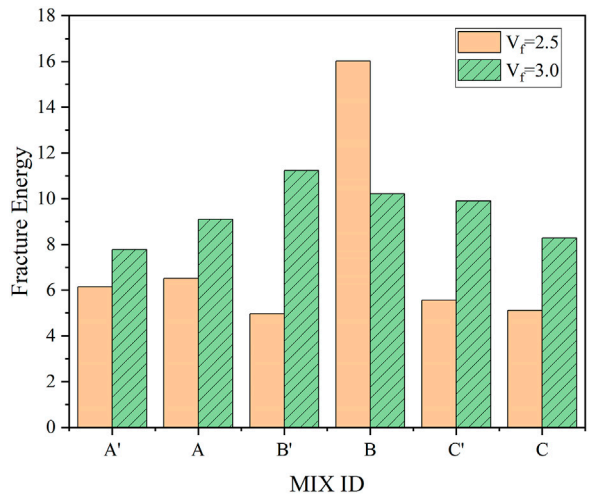

FIGURE 6
Fracture energy under different conditions.

4.2 Analysis of axial tension

Stress–strain curves for composites with three different water/binder ratios are shown in Figure 4.

As illustrated in Figure 4, a steady rise in tensile stress value occurred with the increase in strain until the first crack appeared. At peak stress, the microcrack opening displacement increased. Further loading beyond peak strain caused the cracks to widen. Mixes with a water/binder ratio of 0.30 had a higher fracture energy than those with a water/binder ratio of 0.40 or 0.25. The peak tensile stress of mix B′-3.0 reached 4.89 MPa, and the peak strain of mixes B′-3.0 and B-2.5 reached 3.6% and 3.8%, respectively, which indicates that significant toughness was attained. However, for mix B′-3.0, the strain-hardening and multiple crack phenomena were not elicited. Therefore, a four-point bending test was conducted to further investigate the toughness of this composite.

4.3 Mechanical properties of PP-SACC materials

The effect of water/binder ratio, aggregate size, and fiber content on axial tensile stress are presented in Figure 5.

As explained in the previous section, among these three factors, water/binder ratio exerted the greatest influence on fluidity, followed by fiber content, whereas the influence of aggregate particle size was the weakest. As seen in Figure 5, axial tensile stress first increased and then decreased as water/binder ratio was increased over the three different values of this variable, reaching a peak at the water/binder ratio of 0.30.

When the water/binder ratio was decreased from 0.40 to 0.30, a more stable three-dimensional spatial support system, established by fibers, was formed, and more energy was consumed when fracture occurred. When this happens, the PP fiber overcomes the strong friction force and is finally pulled out, which increases the fracture energy accordingly. When the water/binder ratio was decreased from 0.30 to 0.25, the PP fibers in the matrix had relatively low fluidity were difficult to disperse; this produced the resulting innate weak spots in the specimen, leading to a decrease in fracture energy and peak stress.

As Figure 5 clearly shows, peak tensile stress across all PP-SACC mixes decreased to varying degrees with an increase in aggregate size. The influence of aggregate size on mixes A′-3.0, A′-2.5, B′-2.5, and C′-3.0 was negligible; however, when aggregate size was increased, peak tensile stress for mixes B-3.0 and C-2.5 decreased by 44.4% and 37.6%, respectively, in comparison with mixes B′-3.0 and C′-2.5.

The effects of aggregate size and fiber content on peak strain were similar. The difference was that the effect of fiber content on peak tensile stress was more obvious than that of aggregate size. Peak tensile stress for mix B′-2.5 decreased by 13.0% with an increase in

TABLE 3 Correlation coefficients of mechanical performance indexes.

Correlation coefficient / Performance index	W/B	Aggregate size	Fiber content
Peak tensile stress	−0.7697	−0.3961	−0.5880
Fracture energy	−0.5507	−0.3460	0.8174
Fluidity	0.8389	0.3727	−0.8790

aggregate size. However, peak tensile stress for group B′-2.5 increased by 32.5% with an increase in fiber content.

Under a given water/binder ratio (0.40, 0.30, or 0.25), increasing the aggregate size may induce additional defects in on the cement matrix, which may contribute to insufficient compactness. In addition, increasing the fiber content may have a positive effect on the mechanical properties of the composite. However, not all fibers are fully aligned in the direction of stress, and the effectiveness of this measure is debatable (Sarmiento et al., 2016).

4.4 Revised gray relational analysis

In order to better understand the toughness of PP-SACC in this study, the area enclosed by the strain corresponding to 50% of the peak strength was calculated; this area was defined as the fracture energy per unit volume. The fracture energy of each mix is shown in Figure 6.

As indicated by the analysis presented above, the tensile performance of PP-SACC materials is controlled by a combination of multiple factors rather than a single factor. This is because tensile performance is influenced by complex material characteristics, particularly in strain-hardening cement-based materials (Lu et al., 2018). Therefore, the gray correlation analysis was employed to further analyze the influence of various factors on tensile performance. Gray correlation analysis is generally used to qualitatively address the issue of whether different factors impact a particular variable and which factor has the greater impact. Deng Julong et al. proposed the gray correlation model, which stipulates that the gray correlation degree is a real number between 0 and 1. However, this model cannot account for positive or negative correlations between factors. The advantages and disadvantages of gray correlation are discussed in Qi et al. (2022), and a revised method for calculation of gray correlation degree is proposed in Li et al. (2022); this involves considering the ratio of slopes corresponding to the time period, which can be used to reflect the degree of correlation between sequences.

The operational method employed in this study was as follows. First, the comparison sequence and the reference sequence were designated as in Yin (2016):

$$\boldsymbol{X_i} = \{x_i(1), x_i(2), \ldots x_i(k), \ldots x_i(n)\}, \tag{1a}$$

$$\boldsymbol{X_0} = \{x_0(1), x_0(2), \ldots x_0(k), \ldots x_0(n)\}. \tag{2a}$$

Let $\alpha = \boldsymbol{x}(\boldsymbol{k}) - \boldsymbol{x}(\boldsymbol{k}-\boldsymbol{1})$, $k = 2,3, \ldots, n$, which represents the slope of X on the interval $[k\text{-}1,k]$. The sequence of slopes of $X0$ and Xi on the interval $[k\text{-}1,k]$ were denoted as:

$$\boldsymbol{K_0} = \{\boldsymbol{k_{01}}, \boldsymbol{k_{02}}, \ldots, \boldsymbol{k_{0\,(n-1)}}\}, \tag{3a}$$

$$\boldsymbol{K_i} = \{\boldsymbol{k_{i1}}, \boldsymbol{k_{i2}}, \ldots, \boldsymbol{k_{i\,(n-1)}}\}. \tag{4a}$$

The sequence composed of the ratio of the slopes at the corresponding time periods of ***X0*** and ***Xi*** was denoted as:

$$\boldsymbol{K_{0i}} = K\left\{\frac{\boldsymbol{X_0}}{\boldsymbol{X_i}}\right\} = \left\{k_{01}/k_{i1}, k_{02}/k_{i2}, \ldots, k_{0\,(n-1)}/k_{i\,(n-1)}\right\}. \tag{5a}$$

The coefficient of variation ***K0*** and the generalized coefficient of variation $\boldsymbol{K_{0i}}$ were defined as follows:

$$\delta(\boldsymbol{X_0}) = \frac{S_0}{\overline{K_0}}, \tag{6a}$$

$$\xi(\boldsymbol{X_0}/\boldsymbol{X_i}) = \frac{S_{0i}}{\overline{K_{0i}}}, \tag{7a}$$

where

$$\overline{K_0} = \frac{1}{n-1}\sum_{j=1}^{n-1} k_{0j}, \tag{8a}$$

$$S_0 = \sqrt{\frac{1}{n-2}\sum_{j=1}^{n-1}\left(k_{0j} - \overline{K_0}\right)^2}, \tag{9a}$$

$$\overline{K_{0i}} = \frac{1}{n-1}\sum_{j=1}^{n-1}\left(k_{0j}/k_{ij}\right), \tag{10a}$$

$$S_{0i} = \sqrt{\frac{1}{n-2}\sum_{j=1}^{n-1}\left(k_{0j}/k_{ij} - 1\right)^2}. \tag{11a}$$

The gray correlation degree between ***X0*** and ***Xi*** was defined as follows:

$$\gamma(\boldsymbol{X_0}, \boldsymbol{X_i}) = \begin{cases} \dfrac{1+|\delta(\boldsymbol{X_0})|}{1+|\delta(\boldsymbol{X_0})|+|\xi(\boldsymbol{X_0}/\boldsymbol{X_i})|}\ \overline{K_{0i}} \geq 0, \\ -\dfrac{1+|\delta(\boldsymbol{X_0})|}{1+|\delta(\boldsymbol{X_0})|+|\xi(\boldsymbol{X_0}/\boldsymbol{X_i})|}\ \overline{K_{0i}} < 0. \end{cases} \tag{12a}$$

The values of fluidity, initial cracking strength, and ultimate strength were set as the parent sequence, and water/cement ratio, aggregate particle size, and fiber content were considered as the subsequence. The correlations between each influencing factor and bending performance index are presented in Table 3.

In Table 3, it can be seen that water/cement ratio and fiber content had the greatest impact on peak tensile strength, with both showing a negative correlation. Fiber content had the greatest impact on fracture energy, with an influence factor of 0.8174, followed by water/cement ratio, with an influence factor of −0.5507. Fiber content and water/cement ratio had the greatest impact on flowability. In contrast, the impact of aggregate particle size on peak tensile strength, fracture energy, and flowability was the smallest.

TABLE 4 Parameters a_1, a_2 for each mix.

Mix ID	a_1	a_2	Adj. R-square
A′-2.5	1.20	1.80	0.938
A′-3.0	1.21	1.48	0.910
A-2.5	1.20	1.60	0.972
A-3.0	1.20	1.25	0.906
B′-2.5	1.21	2.40	0.900
B′-3.0	1.22	1.60	0.912
B-2.5	1.21	2.35	0.985
B-3.0	1.22	1.93	0.937
C′-2.5	1.22	2.70	0.944
C′-3.0	1.24	2.39	0.901
C-2.5	1.22	2.60	0.957
C-3.0	1.24	2.35	0.947

In fact, with an increase in water/cement ratio, the amount of water used in the PP-SACC matrix increases and workability is improved. At the same time, the fibers can be fully wrapped by the matrix, but frictional bonding between the PP fibers and the matrix is reduced, which in turn reduces the bridging effect of the fibers and thus affects the tensile properties of the PP-SACC. The influence of PP fiber content on material strength is dialectical. With a decrease in water/cement ratio, more energy is consumed in fiber extraction. PP fibers need to overcome greater frictional force and are eventually pulled out, thus increasing the fracture energy. However, when the water/cement ratio is further reduced, PP fibers are not easily dispersed in a matrix with relatively low flowability, which is the reason for the initial defects occurring in the specimens.

4.5 Axial tensile constitutive model for PP-SACC materials

Guo Zhen Hai (1997) proposed a piecewise function for the complete stress–strain curve of detailed reads, as follows:

$$\begin{cases} y = \alpha x + (1.5 - 1.25\alpha)x^2 + (0.25\alpha - 0.5)x^6 & x \le 1 \\ y = \dfrac{x}{\alpha_t (x-1)^{\beta} + x} & x \ge 1 \end{cases} \tag{1b}$$

$$x = \frac{\varepsilon}{\varepsilon_t} \tag{2b}$$

$$y = \frac{\sigma}{f_t} \tag{3b}$$

where ε and σ are tensile strain and tensile stress, respectively; f_t is the peak tensile stress; and the corresponding strain is ε_t.

Here, the axial tensile constitutive model is obtained with reference to Guo Zhen Hai's equation. The equation should meet the boundary conditions of the ascending and descending portions. The conditions to be fulfilled by the stress–strain equation are:

at $x = 0$, $y = 0$,

at $x = 1$, $y = 1$.

At $0 \le x < 1$, $\frac{d^2y}{dx^2} < 0$, the ascending portion is convex, and the slope is 0 at the peak. At $x \ge 1$, $\frac{d^2y}{dx^2} = 0$, the descending portion has an inflection point. At $x \ge 1$, $\frac{d^3y}{dx^3} = 0$, the descending portion has a maximum curvature point.

For the ascending portion ($0 \le x < 1$), the polynomial function is as follows:

$$y = \alpha_1 x + \alpha_2 x^2 + \alpha_3 x^6 \tag{4b}$$

Using the aforementioned conditions, the equation can be expressed as:

$$y = \alpha_1 x + (1.5 - 1.25\alpha_1)x^2 + (0.25\alpha_1 - 0.5)x^6. \tag{5b}$$

For the descending portion ($x \ge 1$), the rational function is:

$$y = \frac{x}{\alpha_2 (x-1)^{\beta} + x}. \tag{6b}$$

According to the measured stress–strain curves, the formulae for the parameters α_1, α_2, where parameter α_1 corresponds to the ratio of the elasticity modulus at the origin of E_0 to the tangent elasticity modulus at the peak point of E_p,are determined by fitting the test data; these are presented in Table 4.

Based on the significance of the aforementioned parameters, the influence of fiber content (V_f) and water/binder ratio (W/B) on α_1, α_2 is explored by proposing the model shown in Eqs 7b, 8b, as follows:

$$\alpha_1 = P_2 + P_1 \frac{V_f}{W/B}, \tag{7b}$$

$$\alpha_2 = P_1 \frac{B}{WV_f}. \tag{8b}$$

Aggregate size is not considered because its influence on parameters P1 and P2 is negligible. A regression analysis was performed to tease out the relationship between α_1, α_2 and V_f, W/B; this is shown in Figures 7A, B and Table 5.

The parameters can be expressed as follows:

The ascending portion parameter $\alpha_1 = 1.155 + 0.0068 \frac{V_f}{W_B}$.

The descending portion parameter $\alpha_2 = 1.699 \frac{B}{WV_f}$.

A comparison between the theoretical and the experimentally measured curve is depicted in Figures 7C, D. The axial tensile constitutive model coincides well with the experimental results.

4.6 Four-point bending test

In Section 4.3, the influence of water/binder ratio, aggregate size, and fiber content on tensile mechanical properties was discussed. The results obtained for axial tension showed that the B′-3.0 mix demonstrated the best mechanical properties. Therefore, a four-point bending test of composite B′-3.0 was conducted to confirm its toughness. Load value–deflection curves for B′-3.0 are presented in Figure 8.

During the four-point bending test, the first crack was observed on the tensile face in the mid-span of the specimens. As flexural stress increased, multiple cracks with small spacing and tight widths developed and propagated from the first cracking point. When the fiber bridging strength had reached its ultimate strength, bending failure occurred at the corresponding part of the ECC specimen. The deflection curves for mix B′-3.0 are characterized by an initial linear

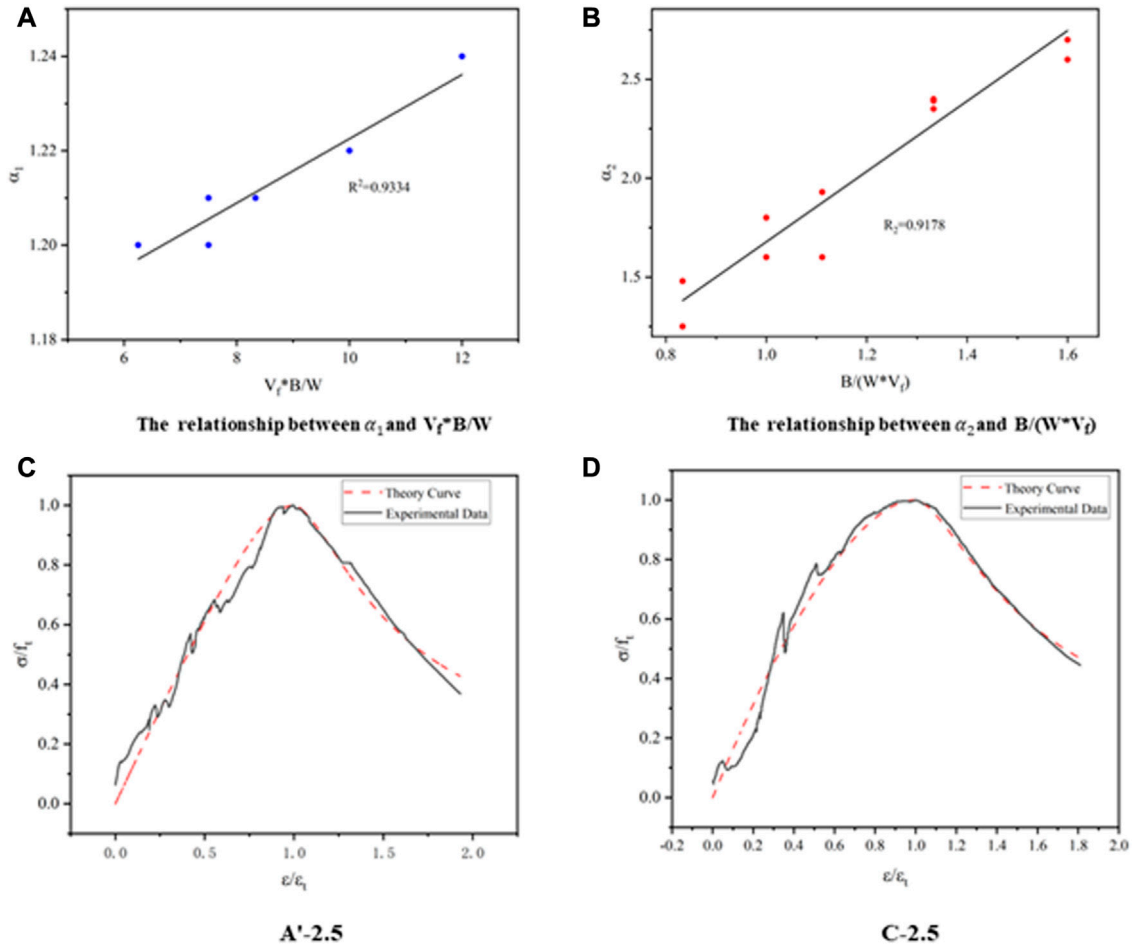

FIGURE 7
Regression analysis of parameters a_1, a_2 **(A,B)** and comparison between the theoretical curve and the measured curve **(C,D)**.

TABLE 5 Regression analysis of a_1, a_2.

Parameter	a_1	a_2
P1	0.0068	1.6990
P2	1.1550	

curve up to the cracking strength, followed by a bend and subsequent plateau, with a relatively small hardening modulus until final fracture. The non-linear portion of the deflection curve corresponds to the continuous microcracking process of the specimens. These curves indicate that the flexural strength of fiber-reinforced sheets is much greater than that of an ordinary cementitious sheet, and there is a longer ductile region.

After reaching ultimate deformation, the specimens were unloaded and removed from the test machine. Upon unloading, the crack characteristics were analyzed using an optical microscope with a maximum magnification of ×100. Only cracks with a width greater than 0.02 mm were recorded due to the limitations of accuracy. After ultimate deformation, all crack widths were less than 1 mm. Due to the high bending ductility of PP-SACC, the

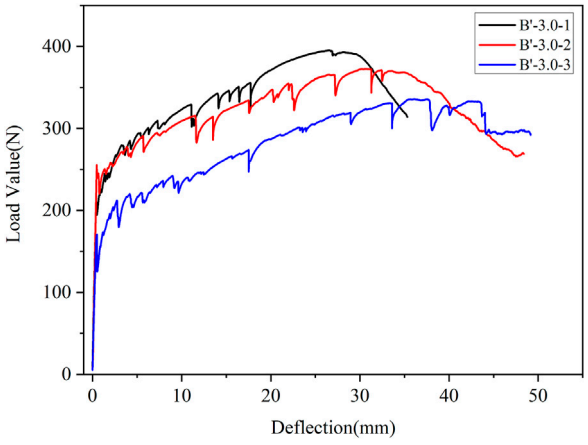

FIGURE 8
Load–deflection curve of B′-3.0.

specimen was still in the deformation strengthening stage when it was loaded, and displacement reached 30 mm, showing microcrack damage. As shown in Figure 9, composite B′-3.0 demonstrated

FIGURE 9
The cracks after unloaded.

TABLE 6 Toughness index of B′-3.0.

Mix ID	I_5	I_{10}	I_{20}	I_{165}
B′-3.0	4.33	8.77	18.65	204.91

steady-state multiple cracking and tight cracks with control performance under the bending load. The average number of cracks was up to 11.7, while the average crack width was only 0.2 mm.

Bend ductility is one of most the important indexes used to evaluate the bending properties of materials. CECS13:2009 defines it as follows: first crack = the point on the load–deflection curve at which the form of the curve first becomes non-linear (approximates the onset of cracking in the concrete matrix); toughness index (I_n) = the number obtained by dividing the area up to a deflection of (n+1)/2 times the first-crack deflection (δc) by the area up to the first crack. These indices reflect the ratio of the energy dissipation of PP-SACC at a specified deflection to the energy dissipation at cracking, and are summarized in Table 6.

The experimental results for the flexural toughness index of each of the specimens are presented in Table 5. The flexural toughness index I_5 of the specimens of PP fiber-reinforced sulfoaluminate cementitious composite was considerably larger than that of the ordinary cementitious specimens. The results of the four-point bending test and axial tension test show that PP-SACC has high toughness, high strength, and excellent crack width control in the case of the B′-3.0 composite.

5 Discussion

Due to the significant influence of water/cement ratio on the flowability of the mortar, flowability increases with an increase in water/cement ratio. When the water/cement ratio is high, the polypropylene (PP) fibers are wetted by the matrix and form good bonds with the fibers. However, a high water/cement ratio also reduces the frictional bond between the PP fibers and the matrix. Moreover, when flowability is low, an insufficient matrix volume can lead to a decrease in fiber bonding performance due to inadequate wetting and bonding of the fibers. As the water/cement ratio increases, the water usage of the PP-sulfate aluminum cement composite (PP-SACC) matrix increases and workability improves, which allows the fibers to be fully wrapped by the matrix. However, this also reduces frictional bonding between the PP fibers and the matrix, resulting in a decrease in the bridging effect of the fibers and affecting the bending performance of the PP-SACC. The effect of PP fiber content on the strength of the material is dialectical. As the water/cement ratio decreases, more energy is consumed when the fiber is pulled out because the fibers need to overcome greater frictional forces. This ultimately increases the fracture energy. However, when the water/cement ratio further decreases, the PP fibers are not easily dispersed in a matrix with relatively low flowability, which is the reason for the initial defects in the sample.

Currently, ordinary Portland cement is the most common form of cement used in cement-based repair materials, which leads to long repair cycles and prolonged maintenance times. Sulfate aluminum cement has significant advantages in repair construction due to its early strength and rapid hardening characteristics. However, due to its rapid development in terms of elastic modulus, cracking often occurs shortly after construction. PP fibers, as a relatively inexpensive and practical modification component, have significant advantages in inhibiting shrinkage and improving toughness. However, there are still relatively few studies on PP fiber-reinforced sulfate aluminum cement, and research on the extent to which performance indicators are affected by multiple factors and the mechanisms underlying these effects is incomplete and not systematic. Therefore, this study combined relatively inexpensive PP fibers with rapid-hardening sulfate aluminum cement to prepare PP-SACC repair materials and optimized the mix ratio for both strength and toughness. The optimized material achieves flexural hardening and a stable tensile strain of more than 3% in performance. The cost of raw materials is significantly reduced, representing an effective promotion for the application of PP-SACC repair materials.

6 Conclusion

Based on the axial tensile test of the PP-SACC material and the four-point bending test, the mechanical properties of PP-SACC material under different PP fiber content levels, aggregate particle sizes, and water/binder ratios were explored. The following conclusions can be drawn.

- The most important factors affecting fluidity are water/binder ratio and fiber content. With an increase in water/binder ratio and a decrease in fiber content, the fluidity of PP-SACC can be significantly increased. However, the influence of aggregate

size on fluidity is the weakest: fluidity only slightly increases with an increase in aggregate size.

- With a decrease in water/binder ratio, the peak tensile stress of PP-SACC first increases and then decreases, reaching its maximum at a water/binder ratio of 0.30. The influence of aggregate size and fiber content on peak strain is similar. With an increase in aggregate size and fiber content, peak tensile stress decreases. The difference between the two is that the influence of fiber content on peak tensile stress is clearer than that of aggregate size. The peak tensile stress of B′-2.5 decreases by 13.0% with an increase in aggregate size, but increases by 32.5% with an increase in fiber content.
- The influence of water/binder ratio, aggregate size, and fiber content on the mechanical properties of PP-SACC was investigated via revised gray relational analysis. The results indicated that water/binder ratio and fiber content can significantly affect peak tensile stress. The most important factor affecting fracture energy is fiber content. In contrast, the influence of aggregate size on peak tensile stress, fracture energy, and fluidity was slight.
- Based on analysis of the axial tensile stress–strain curve, the equation of the PP-SACC axial tensile stress–strain curve in terms of water/binder ratio and fiber content was established, and the axial tensile constitutive model was found to fit the test curve better.
- Considering the axial tensile properties, four-point bending performance, crack number, and crack width of the PP-SACC material, the optimal design for repair materials was determined to be the B′-3.0 composite. B′-3.0 has high toughness, high strength, and provides excellent crack width control, under which peak strain can reach 3.6%.

Data availability statement

The original contributions presented in this study are included in the article/supplementary material, and further inquiries can be directed to the corresponding author.

Author contributions

WX, XX, and CX contributed to the conception and design of the study. FT organized the database. QM performed the statistical analysis. XX wrote the first draft of the manuscript. HL, LL, and GQ wrote sections of the manuscript. All authors contributed to manuscript revision and read and approved the submitted version.

Funding

The authors thank the National Natural Science Foundation of China (under Grant No. 51678492), the Chengdu Science and Technology Project (under Grant No. 2021-YF05-00138-SN), the Fundamental Research Funds for the Central Universities (under Grant No. 2682021GF020), the National Key Research and Development Program of China (under Grant No. 2017YFB1201204), and the Sichuan Province Science and Technology Project (under Grant Nos 2018FZ0095 and 2019YFG0258) for the support of this research.

Conflict of interest

Authors WX, CX, FT, QM, HL, LL, and GQ were employed by China Nuclear Industry Huachen Construction Engineering Co., Ltd.

The remaining author declares that the research was conducted in the absence of any commercial or financial relationships that could be construed as a potential conflict of interest.

Publisher's note

References

Abu Aisheh, Y. I., Atrushi, D. S., Akeed, M. H., Qaidi, S., and Tayeh, B. A. (2022). Influence of steel fibers and microsilica on the mechanical properties of ultra-high-performance geopolymer concrete (UHP-GPC). *Case Stud. Constr. Mater.* 17, e01245. ISSN 2214-5095. doi:10.1016/j.cscm.2022.e01245

Abu Aisheh, Y. I., Atrushi, D. S., Akeed, M. H., Qaidi, S., and Tayeh, B. A. (2021). Influence of polypropylene and steel fibers on the mechanical properties of ultra-high-performance fiber-reinforced geopolymer concrete. *Case Stud. Constr. Mater.* 17, e01234. doi:10.1016/j.cscm.2022.e01234

Afroughsabet, V., Biolzi, L., and Ozbakkaloglu, T. (2016). High-performance fiber-reinforced concrete: A review. *J. Mater. Sci.* 51 (14), 6517–6551. doi:10.1007/s10853-016-9917-4

Belaidi, A. S. E., Benabed, B., and Soualhi, H. (2015). Physical and mechanical properties of concrete repair materials in dry and hot-dry environment. *J. Adhesion Sci. Technol.* 29 (6), 543–554. doi:10.1080/01694243.2014.998001

Boulekbache, B., Hamrat, M., and Chemrouk, M. (2010). Flowability of fibre-reinforced concrete and its effect on the mechanical properties of the material. *Constr. Build Mater.* 24 (9), 1664–1671.

Cai, G. C., and Zhao, J. (2016). Application of sulphoaluminate cement to repair deteriorated concrete members in chloride ion rich environment-A basic experimental investigation of durability properties. *KSCE J. Civ. Eng.* 20 (7), 2832–2841. doi:10.1007/s12205-016-0130-4

Cao, Q., Li, H., and Lin, Z. (2020). Effect of active confinement on compressive behavior of glass fiber-reinforced polymer-confined expansive concrete under axial cyclic loading. *ACI Struct. J.* 117 (1), 207–216.

Chen, K., Wu, D., Yi, M., Cai, Q., and Zhang, Z. (2021) Mechanical and durability properties of metakaolin blended with slag geopolymer mortars used for pavement repair. *Constr. Build. Mater.* 281(2):122566–566. doi:10.1016/j.conbuildmat.2021.122566

Ehrenbring, H. Z., Van den Boogaard, O. Q. A., Liu, X., and Gao, X. (2022). Bending behavior of engineered cementitious composites (ECC) with different recycled and virgin polymer fibers. *Constr. Build. Mater.* 346, 128355. doi:10.1016/j.conbuildmat.2022.128355

Elsanadedy, H. M., Abbas, H., Almusallam, T. H., and Al-Salloum, Y. A. (2019). Organic versus inorganic matrix composites for bond-critical strengthening applications of RC structures – state-of-the-art review. *Compos. Part B Eng.* 174, 106947. doi:10.1016/j.compositesb.2019.106947

He, H., Yang, R., and Wen, J. (2019). Study on the rapid hardening sulphoaluminate-based engineered cementitious composites reinforced with PVA fiber. *Bull. Chin. Ceram. Soc.* 38 (05), 1484–1490.

Hou, M., Zhang, D., and Li, V. C. (2022). Material processing, microstructure, and composite properties of low carbon Engineered Cementitious Composites (ECC). *Cem. Concr. Compos.* 134, 104790. doi:10.1016/j.cemconcomp.2022.104790

Hu, F., Liu, G., and Bi, Y. (2019). Bond properties between micro-steel-fiber reinforced fast hardening high sulphoaluminate cement mortar and steel bar. *Constr. Technol.* 48 (02), 121–125.

Kang, C., Huh, J., Tran, Q. H., and Kwak, K. (2018). Evaluation of self-healing performance of PE and PVA concrete using flexural test. *Adv. Mater. Sci. Eng.* 2018, 1–10. doi:10.1155/2018/6386280

Kong, F., Xu, F., Xiong, Q., Xu, S., Li, X., Fu, W., et al. (2022). Experimental research on properties of UHPC based on composite cementitious materials system. *Coatings* 12 (8), 1219. doi:10.3390/coatings12081219)

Lee, S. (2021) Mechanical properties and durability of mortars made with organic-inorganic repair material. *J. Test. Eval.* 49 (6), JTE20200024. doi:10.1520/JTE20200024

Li, J., Cheng, J., Guo, H., Huang, J., and Yang, J. (2022). Study on influencing factors of supercritical fluid heat transfer coefficient based on grey correlation degree. *Hubei Electr. Power* 46 (1), 7. (In Chinese).

Li, W. (2018). *Study on the application of fiber cement-based repair materials in erosion of bridge Piers.Master thesis*. southwest jiaotong university.

Lu, C., Li, V. C., and Leung, C. K. Y. (2018). Flaw characterization and correlation with cracking strength in Engineered Cementitious Composites (ECC). *Cem. Concr. Res.* 107, 64–74. doi:10.1016/j.cemconres.2018.02.024

Qi, Z., Huang, Z., Li, H., Wang, J., Zhang, H., and Liu, H. (2018). Study of flexural response in strain hardening cementitious composites based on proposed parametric model. *Materials* 12 (1), 113. doi:10.3390/ma12010113

Sadrmomtazi, A., and Khoshkbijari, R. K. (2017). Bonding durability of polymer-modified concrete repair overlays under freeze–thaw conditions. *Mag. Concr. Res.* 69 (23-24), 1268–1275. doi:10.1680/jmacr.17.00014

Sakr, M. A., Osama, B., and Korany, T. E. (2021). Modeling of ultra-high performance fiber reinforced concrete columns under eccentric loading. *Structures* 32, 2195–2210. doi:10.1016/j.istruc.2021.04.026

Sarmiento, E. V., Hendriks, M. A. N., Geiker, M. R., and Kanstad, T. (2016). Modelling the influence of the fibre structure on the structural behaviour of flowable fibre-reinforced concrete. *Eng. Struct.* 124, 186–195. doi:10.1016/j.engstruct.2016.05.053

Shilang, X. U., Wang, N., and Yin, S. (2011). Experimental study on flexural characteristics of RC beams strengthened with post-poured ultra high toughness cementitious composites. *J. Build. Struct.* 2011 (09), 115–122.

Siddika, A., Hajimohammadi, A., Mamun, M., Alyousef, R., and Ferdous, W. (2021). Waste glass in cement and geopolymer concretes: A review on durability and challenges. *Polymers* 13 (13), 2071–71. doi:10.3390/polym13132071

Soupionis, G., Georgiou, P., and Zoumpoulakis, L. (2020). Polymer composite materials fiber-reinforced for the reinforcement/repair of concrete structures. *Polymers* 12 (9), 2058–58. doi:10.3390/polym12092058

Tan, G., Wang, R., Li, W., Liu, W., Wang, X., Wei, X., et al. (2023). Durability evaluation of PP-ECC with local superfine sand (SSPP-ECC) serviced in seasonal frozen region. *Constr. Build. Mater.* 366, 130278. doi:10.1016/j.conbuildmat.2022.130278

Tayeh, B. A., Akeed, M. H., Qaidi, S., and Abu Bakar, B. H. (2022b). Ultra-high-performance concrete: Impacts of steel fibre shape and content on flowability, compressive strength and modulus of rupture. *Case Stud. Constr. Mater.* 17, e01615. doi:10.1016/j.cscm.2022.e01615

Tayeh, B. A., Akeed, M. H., Qaidi, S., and Abu Bakar, B. H. (2022a). Influence of microsilica and polypropylene fibers on the fresh and mechanical properties of ultra-high performance geopolymer concrete (UHP-GPC). *Case Stud. Constr. Mater.* 17, e01367. doi:10.1016/j.cscm.2022.e01367

Wang, L., Du, G., and Gao, H. (2020). Application of capillary waterproofing and anti-corrosive coating system in bridge repairing. *China Build. Waterproofing* 2020 (12), 4.

Wu, C., and Li, V. C. (2017). *Thermal-mechanical behaviors of CFRP-ECC hybrid under elevated temperatures*. Engineering: Composites Part B.

Xu, S. L., Zhang, N., and Zhang, X. F. (2012). Flexural behavior of plain concrete beams strengthened with ultra high toughness cementitious composites layer. *Materials&Structures* 45 (6), 851–859. doi:10.1617/s11527-011-9803-0

Xu, S., and Wang, L. (2011). Flexural crack control performance of existing concrete composite beam reinforced by post-poured UHTCC. *China J. Highw. Transp.* 24 (003), 36–43.

Yesudhas Jayakumari, B., and Nattanmai Swaminathan, E. (2023). A review on characteristics studies on carbon nanotubes-based cement concrete. *Constr. Build. Mater.* 367, 130344. doi:10.1016/j.conbuildmat.2023.130344

Yin, Y. (2016). *Grey correlation analysis of factors affecting visual damage inspection of composite materials*. Nanjing University of Aeronautics and Astronautics. Master's thesis.

Yokota, H., Rokugo, K., and Sakata, N. (2008). *Recommendations for design and construction of high performance fiber reinforced cement composites with multiple fine cracks (HPFRCC)*.

Zhang, C., Liu, Y., and Zhang, M. (2021). PP/PVA fiber reinforced sulphoaluminate cement-based rapid repair material. *Bull. Chin. Ceram. Soc.* 2021 (07), 40.

Zhen, L., Huang, L. M., Wang, S. F., Yang, Z. H., and Yu, L. (2021). Using alumina-rich sludge and phosphogypsum manufactures low-CO2 cement. *Constr. Build. Mater.* 288 (2), 123016. doi:10.1016/j.conbuildmat.2021.123016

Nomenclature

ε tensile strain

σ tensile stress

f_t peak tensile stress

ε_t peak tensile strain

V_f PP fiber content

W/B water/binder ratio